Proc. Natl. Acad. Sci. USA
Vol. 92, pp. 1122–1126, February 1995
Immunology

Structural hierarchy in the clustering of HLA class I molecules in the plasma membrane of human lymphoblastoid cells

(antigen presentation/atomic force microscopy/scanning force microscopy/fluorescence resonance energy transfer/electron microscopy)

SÁNDOR DAMJANOVICH*†, GYÖRGY VEREB*†, ACHIM SCHAPER*, ATTILA JENEI†, JÁNOS MATKÓ†, J. P. PASCUAL STARINK*, GEOFFREY Q. FOX‡, DONNA J. ARNDT-JOVIN*, AND THOMAS M. JOVIN*§

*Department of Molecular Biology and ‡Electron Microscopy Group, Max Planck Institute for Biophysical Chemistry, Postfach 2841, D-37018 Göttingen, Germany; and †Department of Biophysics, University Medical School of Debrecen, Pf. 3., H-4012 Debrecen, Hungary

Communicated by Tibor Farkas, Hungarian Academy of Sciences, Szeged, Hungary, November 7, 1994

ABSTRACT **Major histocompatibility complex (MHC) class I antigens in the plasma membranes of human T (HUT-102B2) and B (JY) lymphoma cells were probed by immunochemical reagents using fluorescence, transmission electron, and scanning force microscopies. Fluorescent labels were attached to monoclonal antibodies W6/32 or KE-2 directed against the heavy chain of HLA class I (A, B, C) and L368 or HB28 against the β_2-microglobulin light chain. The topological distribution in the nanometer range was studied by photobleaching fluorescence resonance energy transfer (pbFRET) on single cells. A nonrandom codistribution pattern of MHC class I molecules was observed over distances of 2–10 nm. A second, nonrandom, and larger-scale topological organization of the MHC class I antigens was detected by indirect immunogold labeling and imaging by transmission electron microscopy (TEM) and scanning force microscopy (SFM). Although some differences in antigen distribution between the B- and T-cell lines were detected by pbFRET, both cell lines exhibited similar clustering patterns by TEM and SFM. Such defined molecular distributions on the surfaces of cells of the immune system may reflect an underlying specialization of membrane lipid domains and fulfill important functional roles in cell–cell contacts and signal transduction.**

The plasma membrane of lymphocytes accommodates many transmembrane proteins, receptors, and antigens, which have a limited mobility and/or occur in oligomeric assemblies (1). Multisubunit structures of key receptors involved in lymphocyte activation, like those of the T-cell receptor-CD3 and the interleukin 2 (IL-2) receptor systems, have been observed (2–5). It is likely that clustering of receptors in the membrane, either preexisting or induced by specific ligands, is important not only in transmembrane signaling but also in antigen presentation and cell–cell communication and contact. Seemingly unrelated integral membrane proteins exhibit a nonrandom pattern of codistribution, as detected by flow cytometric fluorescence energy transfer (FCET), microscope-based photobleaching resonance energy transfer (pbFRET), and lateral mobility measurements or biochemical crosslinking experiments (2, 6–19). Biochemical crosslinking and quantitative FRET can probe the lateral distribution pattern of cell surface antigens and receptors over distances of 2–10 nm (20–26). Recently, a model based on normalized FCET measurements was proposed for the two-dimensional lateral organization of the intercellular adhesion molecule 1 (ICAM-1) molecule, the IL-2 receptor, and the class I and class II human leukocyte antigen (HLA) molecules (2).

The long-range lateral distribution of labeled antigens in the plasma membrane can be detected by electron microscopy and scanning force microscopy (SFM). The latter technique provides a tool for investigation of the surface topography at the air–solid or liquid–solid interface, suitable for imaging with high spatial resolution living and fixed cells in their natural environment (27–33). In this study, we used SFM in parallel with pbFRET and transmission electron microscopy (TEM) to investigate the distribution of major histocompatibility complex (MHC) class I antigens, key molecules in antigen presentation and cell-mediated cytotoxicity. We selected T-cell and B-cell lymphoma lines that express over a million copies of the HLA class I molecules in their plasma membranes.

MATERIALS AND METHODS

Cell Lines. The HUT-102B2 cell line, originally derived from a human adult T lymphoma, was cultured and labeled as described (8). The JY cells, from a human B lymphoma line, were similarly cultured in RPMI-1640 medium supplemented with 10% fetal calf serum and antibiotics (9).

Monoclonal Antibodies (mAbs). The mAbs were W6/32 (IgG2a; a kind gift from F. Brodsky, University of California, San Francisco) and KE-2 (IgG2aκ; the generous gift of M. Edidin, Johns Hopkins University), competing for nearly identical epitopes of the heavy chains of HLA-A, -B, and -C; and L368 (IgG1κ) and HB28 (IgG2b) (provided by M. Edidin and F. Brodsky, respectively), directed against the light chain [β_2-microglobulin (β_2m)]. The antibodies were labeled with fluorescein isothiocyanate (FITC) and tetramethylrhodamine isothiocyanate (TRITC) (Molecular Probes) as described (9). The dye/protein molar ratios varied between 2:1 and 4:1 and were separately determined for each labeled aliquot by spectrophotometric and spectrofluorimetric measurements (9). The Fab fragments were prepared from the mAb by papain digestion and were labeled by FITC and TRITC, as described (34). Dye/protein ratios, determined as for the whole antibodies, varied between 0.8:1 and 1:1.

Cell Labeling Procedures. Cells were harvested and fixed before, or in a number of cases after, the labeling procedure in 0.5% paraformaldehyde for 1 hr at 4°C. After washing the cell suspension twice in phosphate-buffered saline (PBS, pH 7.4), the cell pellet was suspended in 100 μl of PBS and labeled by incubation for 1 hr at 4°C with 10 μg of FITC- or TRITC-conjugated mAb. Labeled cells were washed twice in PBS and fixed in 0.5% paraformaldehyde. For SFM and TEM, the cell suspension was further incubated with 10 μl of Aurogamig G-30 (Amersham; diameter, 30 ± 3 nm) or 10 μl of gold-labeled Gamig

The publication costs of this article were defrayed in part by page charge payment. This article must therefore be hereby marked "*advertisement*" in accordance with 18 U.S.C. §1734 solely to indicate this fact.

Abbreviations: HLA, human leukocyte antigen; MHC, major histocompatibility complex; pbFRET, photobleaching fluorescence resonance energy transfer; TEM, transmission electron microscopy; SFM, scanning force microscopy; FITC, fluorescein isothiocyanate; TRITC, tetramethylrhodamine isothiocyanate; mAb, monoclonal antibody; β_2m, β_2-microglobulin.

§To whom reprint requests should be addressed.

G-15 (Biotrends, Cologne, Germany; diameter, 15 ± 2 nm) carrying polyclonal goat anti-mouse antibodies, directed against the IgG Fc or whole molecule, respectively. After a 1-hr incubation on ice the cells were washed and stored at 4°C.

Photochemical Immobilization of Cells on Coverslips. Photochemical crosslinking (29, 32) of the cells to a glass support with *N*-(5-azido-2-nitrobenzoyloxy)succinimide (ANB-NOS) was carried out according to Henderson (31). Washed and chemically etched coverslips were derivatized with 3-aminopropyltriethoxysilane (APTES). Cells were added to a buffer or water droplet placed on the APTES- and ANB-NOS-treated coverslips for 30 min in the dark. The crosslinking moieties were photoactivated with 366-nm UV light for 5 min.

pbFRET Measurements. Photobleaching energy transfer measurements were performed as described (refs. 21–23; T. W. J. Gadella and T.M.J., unpublished work). Lymphoid cells were tagged with fluorescently labeled antibodies against surface antigens (see Table 1). Aliquots of 4 μl were placed on poly(L-lysine)-coated microscope slides, covered with round coverslips, and sealed with rubber cement. Appropriate filter and dichroic mirror sets were used to select 485 ± 10 nm excitation and 525 ± 15 nm emission bands. Spatially resolved photobleaching time constants for individual cells were measured on a Zeiss Axioplan microscope. A sequence of 31 10-s exposures was collected from each cell through a 63×, numerical aperature 1.25, Neofluar objective using a Photometrics (Tucson, AZ) cooled scientific charge-coupled device camera (series 200, Kodak KAF1400 sensor) interfaced to a Macintosh Quadra 800 computer (Apple Computer). The sequences were processed on a VAX workstation with macros implemented in TCL-Image (TPD, University of Delft, Delft, The Netherlands) image-processing routines and a Fortran exponential-fitting program (ref. 23; T. W. J. Gadella and T.M.J., unpublished work). Bleaching time constants (τ_{bl}) of donor only (τ_d) or donor and acceptor ($\tau_{d,a}$) labeled cells were calculated for every pixel in the image and energy transfer efficiencies were calculated as ET (%) = $100 \cdot [1 - (\tau_d/\tau_{d,a})]$ (21).

SFM. A NanoScope III contact SFM (Digital Instruments, Santa Barbara, CA) was operated in the constant force (images shown in Fig. 2) or deflection modes in air and in liquid with a fluid cell (Digital Instruments). Si_3N_4 cantilevers with integrated pyramidal tips (Digital Instruments) were used with a spring constant of about 0.06 N/m. Scanning was with a J-tube transducer [128 × 128 μm (x, y) and 5.6-μm (z) scan range; calibration is discussed in ref. 35]. The scan rate was 6 lines per s. Images (512 × 512 pixels) were processed with the NanoScope software including plane fitting and flattening and cross-sectional analysis of the gold particles.

The constant force SFM images were filtered and the curvature of the tip was estimated using digital smoothing filters (J.P.P.S. and T.M.J., unpublished work). The most probable position of the tip was estimated at each point of the image using a parabolic model for the local contact area between the tip and the sample. Each pixel value (corresponding to an apparent height value) was corrected by the computed z-axis displacement from the estimated nonapical contact point to the corresponding position of the apex. During the final reconstruction of the surface envelope, the material overlapping the tip was removed computationally [exclusion principle (36)].

TEM. TEM was performed on a JEOL-100 B electron microscope operated at 100 kV. Gold-labeled HUT-102B2 and JY cells were fixed with 1% glutaraldehyde in 0.1 M sodium cacodylate (pH 7.2) for 1 hr at 4°C. The cells were washed in 0.15 M cacodylate buffer and postfixed in 1% osmium tetroxide buffered in 0.15 M sodium cacodylate for 1 hr at 4°C. After rinsing the cells with buffer they were layered on a wet Millipore filter (0.45 mm) and overlaid with agar (1.5% in water) at 40°C. Agar blocks (2 × 2 × 2 mm) were trimmed and dehydrated in ascending concentrations of ethanol (20–95%), transferred through propylene oxide, and embedded in Epon resin. Thin sections of about 100 nm thickness were sliced and negatively stained with 1% lead citrate and 1% uranyl acetate. Alternatively, the cells were spread on Formvar-coated grids, fixed with 1% glutaraldehyde, and air dried.

Immunogold Particle Analysis. The distribution of the gold particles was analyzed according to Starink *et al.* (37, 38). The procedure combines region growing and edge detection to segment the gold particles, including those in the form of aggregates. For a random distribution of particles, the corresponding distribution r of nearest-neighbor distances should be Poissonian (39). Furthermore, the ratios of the expected mean $E(r)$ to the sample mean $\langle r \rangle$ and of the expected variance $E(s)$ to the sample variance s should be approximately unity.

RESULTS AND DISCUSSION

Short-Range Clustering of HLA Antigens Revealed by pbFRET of Single Cells. The FRET efficiencies were determined between the heavy and light chain of class I HLA molecules of individual cells prepared in the same way as for SFM measurements. The antigens were labeled with mAbs or Fab fragments carrying the fluorescent donor and acceptor groups. The goal of these experiments was to relate the results gained under the present fixation conditions to data from previous

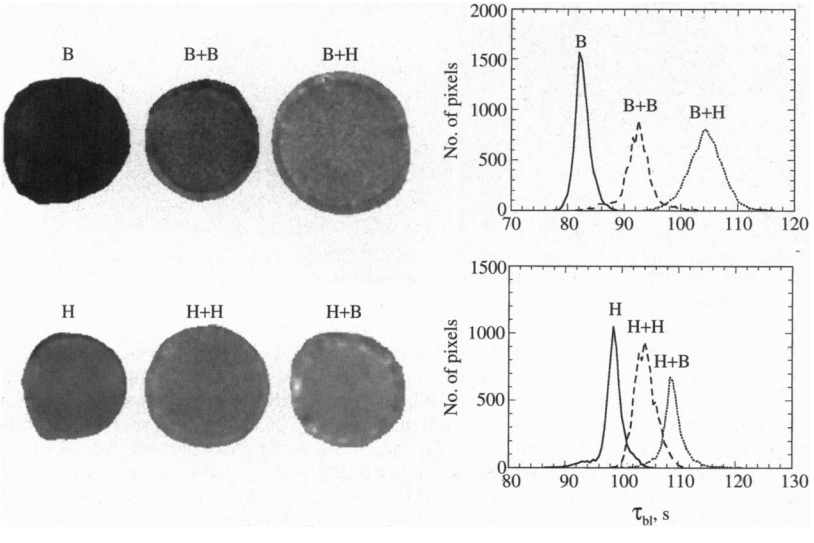

FIG. 1. Molecular proximities of the MHC class I antigens assessed by pbFRET. (*Left*) Images of JY cells in which the photobleaching time constant (τ_{bl}) is represented on a grey scale; lighter tones correspond to higher values. (*Right*) Distribution histograms of τ_{bl} for the same cells. The cells were labeled with fluorescence donor in the form of FITC-conjugated HB28 (B; specific for β_2m) and W6/32 (H; specific for the MHC class I heavy chain) Fab fragments. Simultaneous labeling with a second Fab fragment conjugated with TRITC as the acceptor is represented by +B and +H.

Table 1. Energy transfer efficiencies calculated from pbFRET measurements

Epitope		Ab	ET, %	
Donor	Acceptor	type	T cells	B cells
β_2m	HLA I hc	Fab	15–20	22–27
β_2m	β_2m	Fab	11–13	12–14
HLA I hc	HLA I hc	Fab	6–7	7–8
β_2m	HLA I hc	mAb	9–11	15–17
β_2m	β_2m	mAb	5–6	4–5
HLA I hc	HLA I hc	mAb	7–8	6–7

Energy transfer (ET) values between FITC-labeled donor and TRITC-labeled acceptor mAbs or their papain-digested Fab fragments are shown for T (HUT-102B2) and B (JY) lymphoblastoid cells. Each indicated range represents the mean ± SEM calculated from 10^4–10^5 points in 4–10 independently measured individual cells. The donors and acceptors are specified by the cell surface target epitopes: β_2m and HLA class I heavy chain (HLA I hc), tagged by HB28 and W6/32 antibodies, respectively.

studies and to demonstrate that application of bivalent whole mAbs does not by itself induce clustering of the particular antigens under investigation. The results are summarized in Fig. 1 and Table 1. The intramolecular transfer efficiency between β_2m (light chain) and the heavy chain of the HLA class I antigen (entries 1 and 4) served as positive controls. Significant energy transfer was found between HLA class I heavy chain molecules labeled simultaneously with FITC- and TRITC-conjugated Fab fragments of the W6/32 mAb in equimolar ratios. Therefore, a molecular proximity of the HLA class I A, B, and C heavy chains of both the T and B lymphoma lines can be inferred, presumably arising as a consequence of homoassociation, i.e., antigen clustering. There are an estimated 1.2×10^6 and 1.6×10^6 HLA class I antigens on the surfaces of the HUT-102B2 and JY cells, respectively (2). Assuming a surface area corresponding to a spherical cell 20 μm in diameter, the mean distance between HLA molecules would be about 40 nm for randomly distributed antigens, corresponding to an expected energy transfer efficiency of <2% (40). A somewhat larger energy transfer efficiency was measured with Fab fragments between the β_2m molecules than between the heavy chains of HLA class I for both cell lines (lines 2 and 3 in Table 1).

Since Fab fragments that are monovalent yield transfer efficiencies similar to those with whole antibodies (Table 1), an aggregation of the HLA class I clusters induced by the intact mAbs can be excluded. The results obtained with whole antibodies in these experiments and from previous flow cytometric measurements (2, 8, 9, 12) correlate well.

It is possible that the codistribution pattern of the HLA class I molecules that we observe by pbFRET may modulate the HLA class I-restricted antigen presentation and cell-mediated cytotoxicity. In earlier experiments a similar clustering was observed between HLA class I and class II and between ICAM-1 and IL-2 receptor α subunit (2, 8, 9).

Visualization of Colloidal Gold-Labeled HLA Class I Antigens by SFM in Air and in Liquid. An SFM image of an

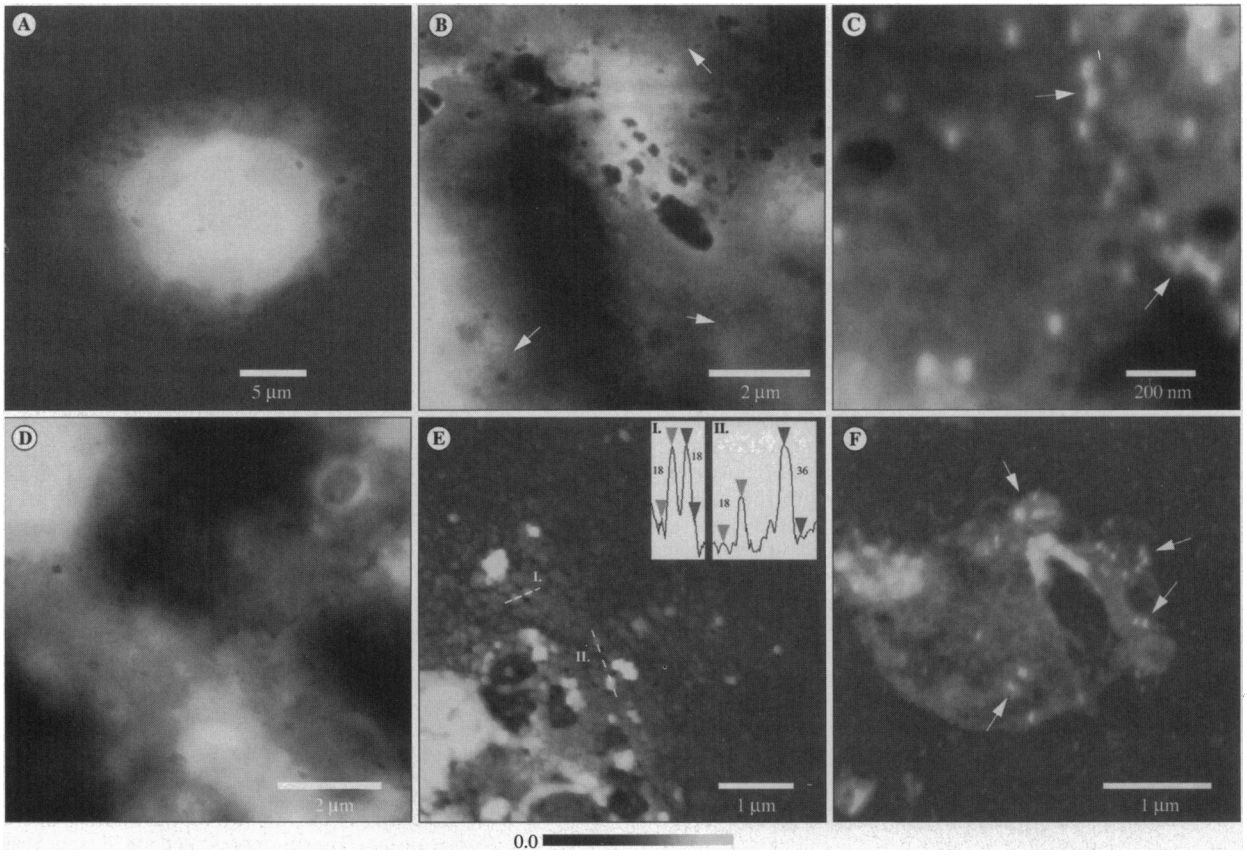

FIG. 2. SFM images of HUT-102B2 T cells with and without gold labels targeted to HLA class I antigens. (*A*) SFM image of a solitary cell. (*B*) Cell labeled first with W6/32 and L368 mAbs to the HLA class I and thereafter with a second antibody carrying the 30-nm diameter gold bead. Arrows point toward apparent clusters. (*C*) Sample as in *B* but at higher resolution. Clustered gold labels are clearly visible (arrows). (*D*) Negative control cell treated only with the second antibody. (*E*) JY cell, double labeled with 30-nm and 15-nm diameter gold beads carrying second antibodies against the primary HLA class I-directed mAbs. The labels are on the cellular membrane but appear on the cover glass support as well (upper, right). (*Inset*) Sections with the indicated trajectories I and II, demonstrating the dimensions of the two differently sized labels along the *z* axis, i.e., perpendicular to the surface. (*F*) Thirty-nanometer diameter gold labels on a fragment of a HUT-102B2 cell membrane scanned in buffer. Arrows point toward apparent clusters. (The bar below codes height information: 3000, 400, 70, 400, 150, and 150 nm in *A*–*F*, respectively.)

air-dried HUT-102B2 cell double labeled with W6/32 and L368, intramolecular mAb pairs for the HLA antigen heavy and light chains, and visualized with colloidal gold-conjugated secondary antibodies is shown in Fig. 2*A*. Under our drying and fixation conditions the lymphoblasts changed to an oblate shape, ≈2.5–3 μm in height and >20 μm in diameter. Usually, the dried cell surface appeared very rough with surface corrugations in the submicron range. One is constrained in classifying surface structures to identification of particles with uniform and narrowly distributed size ranges. Protrusions of about 30 nm in height were apparent on the labeled cells and best visualized on the flattened cell margin (Fig. 2 *B* and *C*). This discrete size range of surface projections was not observable on control cells treated only with the gold-labeled second antibody (Fig. 2*D*). For identification we considered only the height of the gold particle since the lateral bead dimensions were significantly larger due to structural broadening from tip-sample convolution (36, 41–43). As can be seen from Fig. 2*C*, the gold markers often appeared clustered as doublets, triplets, or even higher aggregates. Gold-labeled antibody spread on mica in the absence of cells was free from triplets and contained only a very small number of doublets (data not shown). The images presented are representative of the antigen labeling resolvable by the SFM; similar pictures were seen in the case of labeling with KE-2 or W6/32 antibody alone, on both JY and HUT-102B2 cells. Our results suggest that SFM has the resolving power for visualizing antibody-targeted gold labels on the cell surface of air-dried specimens without further treatment.

Both 15-nm and 30-nm gold particles conjugated with polyclonal antibodies could be resolved by SFM (Fig. 2*E*). A single epitope was allowed to react with whole mAb and subsequently double labeled, with the larger gold conjugates directed to the Fc part of the mouse IgGs and the smaller ones to the whole IgG heavy and light chains. The smaller labels, with an apparent height of 18 nm, were barely discernible among the background grains but were distinguishable from the larger ones of 36 nm apparent height (Fig. 2*E Inset*). The successful labeling of the cells with two different sizes of gold particle in SFM offers the possibility of analyzing heterologous cell surface receptors or antigen populations.

One of the advantages of SFM imaging over conventional electron microscopy is the ability to image nondehydrated objects in their natural (aqueous) environments. Additionally, air-drying of the samples may cause artifactual collapsing of the membrane, leading to compromised data. Photochemical crosslinking of the cells to the substrate (29, 32) guaranteed sufficient cell immobilization provided that the cells were not exposed to strong shearing forces during washing or other treatments. Furthermore, it allowed cell labeling in solution prior to spreading on the coverslips. One such membrane fragment is shown in Fig. 2*F*. The resolution afforded by the gold labels was comparable to that of the dry samples, but, as expected, the cell body was considerably more extended in the *z* direction. The latter phenomenon rendered more difficult the localization of regions of interest for scanning; we have confirmed that the deflection (error) mode of SFM scanning is advantageous for emphasizing structures characterized by steep gradients under these conditions (44, 45).

TEM of Immunogold-Labeled Cells. A TEM micrograph of a membrane surface area at the cell margin of a gold-labeled HUT-102B2 lymphoblast is shown in Fig. 3. Due to their large scattering cross section, the gold markers are visualized with excellent contrast. Fig. 3 *A* and *B* depict samples labeled concurrently with 15-nm and 30-nm colloidal gold markers directed against W6/32 and L368 mAbs bound to MHC class I molecules; similar images were obtained with the larger beads alone (data not shown). A nonrandom distribution pattern of the 30- and 15-nm diameter gold beads was clearly visible. The two-sized beads were colocalized within the groups of clustered particles but demonstrated a tendency to partition, possibly a reflection of preferential size-dependent forces dictating the physical packing in these regions of high antigen density.

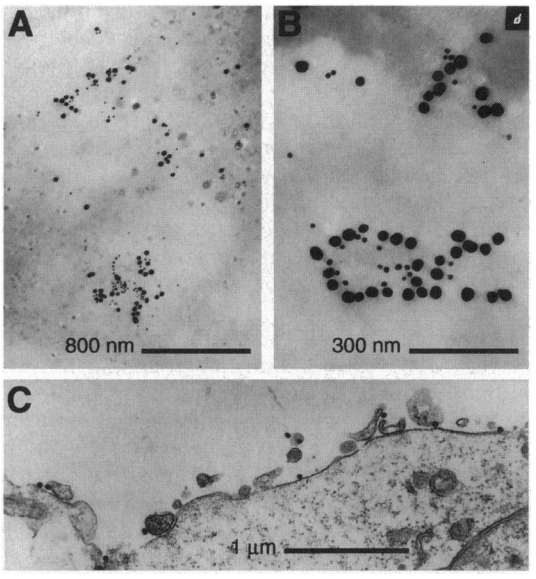

FIG. 3. TEM image of immunogold-labeled HUT-102B2 cells. (*A* and *B*) Membrane surface of a fixed cell on the electron microscope grid at two different resolutions. (*C*) Same cell type after sectioning to 100 nm thickness. The beads are clustered in all cases.

In Fig. 3*C*, gold beads are seen attached to the outer plasma membrane of an embedded and sectioned lymphoblast and distributed in a manner similar to that seen by SFM in Fig. 2*C*. Steric hindrance mediating the gold labeling efficiency is again a critical point with respect to data interpretation, since it appeared that the binding of one kind of bead tended to exclude the other on the 2- to 10-nm length scale characteristic of efficient FRET.

Image Processing Revealed a Nonrandom Distribution of Immunogold Markers in SFM and TEM Micrographs. To derive a more quantitative assessment of the distribution pattern of the gold markers on the plasma membrane, an analysis was undertaken of the interparticle distances in terms of the formalism described in *Materials and Methods*. The ratios of the expected interparticle distance $E(r)$ to the sample mean r and of the corresponding expected variance $E(s)$ to the sample variance s were about 0.6 and 3, respectively, far from the value of unity expected for particles distributed randomly. These results are indicative of clusters superimposed on a uniform background labeling. The mean diameter ± SD of the 43 large gold particles observed in Fig. 3*B* was 36.1 ± 3.6 nm and of the 25 small particles, 15.7 ± 3.6 nm, in good agreement with the manufacturer specifications.

Concluding Remarks. We have employed a number of experimental methods permitting the detection of molecular proximity on different size scales. Photobleaching FRET revealed association of class I MHC molecules at the Å level confirming earlier flow cytometric measurements (2, 8, 9, 12). In addition, it has shown that the applied mAbs do not induce aggregation of the labeled antigens. Owing to the limitations in the resolving power of the conventional microscope, the distribution of the small antigen clusters appeared to be homogeneous; that is, a ring-like fluorescence was observed with the labeled antibodies, and the distribution of fluorescence bleaching time constants was uniform. This alone would speak for "microclustering" at the Å level and homogeneity at the μm level. However, SFM and TEM showed yet another level of association, a "macroclustering" phenomenon, on a

scale of some 10 nm, which could not be resolved by conventional optics in fluorescence microscopy, and which was above the range of efficient resonance energy transfer. Although this grouping of the HLA class I molecules could conceivably reflect a partial loss of gold particles attached to monovalent antigen sites due to shearing forces, there was no decrease in the fluorescence of the primary antibodies indicating such a phenomenon. In addition, preliminary measurements of the rotational diffusion of HLA molecules on JY cells suggest a mean cluster size of 25 monomers on average,[¶] pointing to a possible degree of oligomerization greater than that revealed by FRET.

Taken as a whole, the data suggest a hierarchical arrangement of the MHC class I antigens, consisting of specific patterns of localization but with a degree of randomness in the distribution. The origin of antigen codistribution is uncertain. Interactions operating on the extracellular face of the membrane, within it, and/or in the submembranous (cytosolic) compartment are surely operative, and lipid domain effects have to be considered as well. Interactions of hydrophobic protein domains with their lipid environment, e.g., at the surface of the rough endoplasmic reticulum (46), are well established and predictable. It has been suggested that lipid domains comprise relatively large yet delimited areas based on lateral mobility measurements of defined membrane systems (47). Other levels of organization can be visualized. For example, theoretical considerations lead to the prediction that electrically charged ion channels can form dissipative structures in a fluid membrane, driven by ion concentration gradients (48). Preexisting clusters of receptors and specific antigens, such as those demonstrated in this study, may be crucial to the regulation of intercellular communication in general and the central functions of cellular immunology in particular, such as antigen presentation and the subsequent activation of cytotoxic T lymphocytes (49).

The lateral clustering, i.e., a high local density of class I HLA molecules, may improve the efficiency of antigen presentation by intensifying the avidity of both HLA CD8 and HLA T-cell receptor binding (12), very likely by increasing the multiplicity of low-affinity "vertical" interactions between antigen-presenting cells and cytotoxic T lymphocytes. Similar mechanisms may be operational in the model proposed for the antigen presentation by "dimers of MHC class II dimers" (15, 50). Colocalization of HLA molecules with intercellular adhesion molecules (such as ICAM-1) in these clusters (2) suggests another potential role of clustering. By increasing the local density of adhesion molecules, and thereby the multiplicity of intercellular interactions, clusters may serve to stabilize weak contacts between cells.

The work was supported by the Max Planck Society, by the National Research Fund, Hungary (OTKA Grants 6221 and F-013335 to S.D. and G.V., respectively), and by the German Research Council (DFG Grant Jo 105/9). S.D. was a visiting professor at the Max Planck Institute for Biophysical Chemistry. G.V. is the recipient of a postdoctoral fellowship from the Alexander von Humboldt Foundation.

1. Waldmann, T. A. (1991) *J. Biol. Chem.* **266,** 2681–2684.
2. Bene, L., Balázs, M., Matkó, J., Möst, J., Dierich, M. P., Szöllösi, J. & Damjanovich, S. (1994) *Eur. J. Immunol.* **24,** 2115–2123.
3. Edidin, M. (1988) *Immunol. Today* **9,** 218–219.
4. Edidin, M., Zuniga, M. C. & Scheetz, M. (1994) *Proc. Natl. Acad. Sci. USA* **91,** 3378–3382.

[¶]Matkó, J., Jenei, A., Bene, L., Edidin, M., Jovin, T. M., Szöllösi, J., and Damjanovich, S., International Biophysics Congress, July 25–30, 1993, Budapest, Hungary, abstr. G1.39.

5. Kent, U. M., Mao, S.-Y., Wofsy, C., Goldstein, B., Ross, S. & Metzger, H. (1994) *Proc. Natl. Acad. Sci. USA* **91,** 3087–3091.
6. Damjanovich, S., Trón, L., Szöllösi, J., Zidovetzki, R., Vaz, W. L. C., Regateiro, F., Arndt-Jovin, D. J. & Jovin, T. M. (1983) *Proc. Natl. Acad. Sci. USA* **80,** 5985–5989.
7. Damjanovich, S., Szöllösi, J. & Trón, L. (1992) *Immunol. Today* **13,** A13–A15.
8. Szöllösi, J., Damjanovich, S., Goldman, C. K., Fulwyler, M. J., Aszalós, A., Goldstein, G., Rao, P. & Waldmann, T. A. (1987) *Proc. Natl. Acad. Sci. USA* **84,** 7246–7250.
9. Szöllösi, J., Damjanovich, S., Balázs, M., Nagy, P., Trón, L., Fulwyler, M. J. & Brodsky, F. M. (1989) *J. Immunol.* **143,** 208–213.
10. Mittler, R. S., Goldman, S. J., Spitalny, G. L. & Burakoff, S. J. (1989) *Proc. Natl. Acad. Sci. USA* **86,** 8531–8535.
11. Mittler, R. S., Rankin, B. M. & Kiener, P. A. (1991) *J. Immunol.* **147,** 3434–3440.
12. Matkó, J., Bushkin, Y., Wei, T. & Edidin, M. (1994) *J. Immunol.* **152,** 3355–3360.
13. Liegler, T., Szöllösi, J., Hyun, W. & Goodenow, R. S. (1991) *Proc. Natl. Acad. Sci. USA* **88,** 6755–6759.
14. Matkó, J., Szöllösi, J., Trón, L. & Damjanovich, S. (1988) *Q. Rev. Biophys.* **21,** 479–544.
15. Germain, R. N. (1993) *Curr. Biol.* **3,** 586–589.
16. Chakrabarti, A., Matkó, J., Rahman, N. A., Barisas, G. B. & Edidin, M. (1992) *Biochemistry* **31,** 7182–7189.
17. de la Hera, A., Muller, U., Olsson, C., Isaaz, S. & Tunnacliffe, A. J. (1991) *J. Exp. Med.* **173,** 7–17.
18. Bushkin, Y., Demaria, S., Lee, J. & Schwab, R. (1988) *Proc. Natl. Acad. Sci. USA* **85,** 3985–3989.
19. Szabó, G., Jr., Pine, S. P., Weaver, J. L., Kasari, M. & Aszalós, A. (1992) *Biophys. J.* **61,** 661–670.
20. Chan, S. S., Arndt-Jovin, D. J. & Jovin, T. M. (1979) *J. Histochem. Cytochem.* **27,** 56–64.
21. Jovin, T. M. & Arndt-Jovin, D. J. (1989) in *Cell Structure and Function by Microspectrofluorimetry*, eds. Kohen, E. & Hirschberg, J. G. (Academic, San Diego), pp. 99–115.
22. Jovin, T. M. & Arndt-Jovin, D. J. (1989) *Annu. Rev. Biophys. Biophys. Chem.* **18,** 271–308.
23. Jovin, T. M., Arndt-Jovin, D. J., Marriott, G., Clegg, R. M., Robert-Nicoud, R. & Schormann, T. (1990) in *Optical Microscopy for Biology*, eds. Herman, B. & Jacobson, K. (Wiley–Liss, New York), pp. 575–602.
24. Kubitscheck, U., Schweitzer-Stenner, R., Arndt-Jovin, D. J., Jovin, T. M. & Pecht, I. (1993) *Biophys. J.* **64,** 110–120.
25. Trón, L., Szöllösi, J., Damjanovich, S., Helliwell, S. H., Arndt-Jovin, D. J. & Jovin, T. M. (1984) *Biophys. J.* **45,** 939–946.
26. Young, R. M., Arnette, J. K., Roess, D. A. & Barisas, B. G. (1994) *Biophys. J.* **67,** 881–888.
27. Binnig, G., Quate, C. F. & Gerber, C. (1986) *Phys. Rev. Lett.* **56,** 930–933.
28. Hoh, J. H. & Hansma, P. K. (1992) *Trends Cell Biol.* **2,** 208–213.
29. Karrasch, S., Dolder, M., Schabert, F., Ramsden, J. & Engel, A. (1993) *Biophys. J.* **65,** 2437–2446.
30. Neagu, C., Van der Werf, K. O., Putman, C. A. J., Kraan, Y. M., de Grooth, B. G., van Hulst, N. F. & Greve, J. (1994) *J. Struct. Biol.* **112,** 32–40.
31. Henderson, E. (1994) *Prog. Surf. Sci.* **46,** 39–60.
32. Karrasch, S., Hegerl, R., Hoh, J. H., Baumeister, W. & Engel, A. (1994) *Proc. Natl. Acad. Sci. USA* **91,** 836–838.
33. Pietrasanta, L. I., Schaper, A. S. & Jovin, T. M. (1994) *J. Cell Sci.* **107,** 2427–2437.
34. Edidin, M. & Wei, T. (1982) *J. Cell Biol.* **95,** 458–465.
35. Schaper, A., Wolthaus, L., Mobius, D. & Jovin, T. M. (1993) *Langmuir* **9,** 2178–2184.
36. Keller, D. J. & Franke, F. S. (1993) *Surf. Sci.* **294,** 409–419.
37. Starink, J. P. P. & Young, I. T. (1993) *Pattern Recognition Lett.* **14,** 895–905.
38. Starink, J. P. P., Humbel, B. M. & Verkleij, A. J. (1994) *Biophys. J.*, in press.
39. Schwarz, H. & Exner, H. E. (1983) *J. Microsc. (Oxford)* **129,** 155–169.
40. Jovin, T. M. & Arndt-Jovin, D. J. (1982) in *Trends in Photobiology*, eds. Hélène, C., Charelier, M., Montenay-Garestier, T. & Laustriat, G. (Plenum, New York), pp. 51–66.
41. Keller, D. (1991) *Surf. Sci.* **253,** 353–364.
42. Vesenka, J., Manne, S., Giberson, R., Marsh, T. & Henderson, E. (1993) *Biophys. J.* **65,** 992–997.
43. Bustamante, C., Vesenka, J., Tang, C. L., Rees, W., Guthold, M. & Keller, R. (1992) *Biochemistry* **31,** 23–26.
44. Fritz, M., Radmacher, M. & Gaub, H. E. (1994) *Biophys. J.* **66,** 1328–1334.
45. Putman, C. A. J., van der Werf, K. O., de Grooth, B. G., van Hulst, N. F., Greeve, J. & Hansma, P. K. (1992) *SPIE Proc.* **1639,** 198–204.
46. Hartmann, E. T., Rappoport, A. & Lodish, H. F. (1989) *Proc. Natl. Acad. Sci. USA* **86,** 5786–5790.
47. Edidin, M. (1990) *Curr. Top. Membr. Transp.* **36,** 81–96.
48. Fromherz, P. (1988) *Proc. Natl. Acad. Sci. USA* **85,** 6353–6357.
49. Burton, J., Goldman, C. K., Rao, P., Moos, M. & Waldmann, T. A. (1990) *Proc. Natl. Acad. Sci. USA* **87,** 7329–7333.
50. Brown, J. H., Jardetzky, T. S., Gorga, J. C., Stern, L. J., Urban, R. G., Strominger, J. L. & Wiley, D. C. (1993) *Nature (London)* **364,** 33–39.